PROGRESS IN PHOTOVOLTAICS: RESEARCH & APPLICATIONS
Prog. Photovolt: Res. Appl. 2012; **20**:6–11
Published online 6 September 2011 in Wiley Online Library (wileyonlinelibrary.com). DOI: 10.1002/pip.1160

ACCELERATED PUBLICATION

Device characteristics of a 10.1% hydrazine-processed $Cu_2ZnSn(Se,S)_4$ solar cell

D. Aaron R. Barkhouse†, Oki Gunawan†, Tayfun Gokmen, Teodor K. Todorov and David B. Mitzi*

IBM Thomas J. Watson Research Center, 1101 Kitchawan Rd, Yorktown Heights, NY, 10598, USA

ABSTRACT

A power conversion efficiency record of 10.1% was achieved for kesterite absorbers, using a $Cu_2ZnSn(Se,S)_4$ thin-film solar cell made by hydrazine-based solution processing. Key device characteristics were compiled, including light/dark *J–V*, quantum efficiency, temperature dependence of V_{oc} and series resistance, photoluminescence, and capacitance spectroscopy, providing important insight into how the devices compare with high-performance $Cu(In,Ga)Se_2$. The record kesterite device was shown to be primarily limited by interface recombination, minority carrier lifetime, and series resistance. The new level of device performance points to the significant promise of the kesterites as an emerging and commercially interesting thin-film technology. Copyright © 2011 John Wiley & Sons, Ltd.

KEYWORDS

$Cu_2ZnSn(S,Se)_4$; kesterite; earth abundant; thin-film solar cell; solution processing

***Correspondence**

David B. Mitzi, IBM Thomas J. Watson Research Center, 1101 Kitchawan Rd, Yorktown Heights, NY, 10598, USA.
E-mail: dmitzi@us.ibm.com
†D. A. R. Barkhouse and O. Gunawan contributed equally to this work.

Received 17 February 2011; Revised 13 April 2011

1. INTRODUCTION

Thin-film solar cells show a great deal of promise for converting sunlight to electricity at a cost that is competitive with fossil fuels. However, most thin-film technologies in commercial production today use rare elements, such as indium and tellurium [1,2], which are expected to increase significantly in cost as solar module production rises above ~10GW of peak power capacity per year (GWp/year) [3]. Current global installed electricity generation capacity is in excess of 4TW and is expected to reach 7TW by 2035 [4]. In order to meet this increase in electricity demand while avoiding the worst effects of climate change, it is desirable to have a cost-effective solar energy technology that can support a >100-GWp/year production volume without straining global supplies of any of its constituents. Copper zinc tin sulfide selenide (CZTSSe) solar cells have recently emerged as an attractive candidate [5–9], as they have similar properties with copper indium gallium sulfide selenide (CIGSSe) cells but with the rare and/or expensive indium and gallium replaced with the more common and less expensive zinc and tin, allowing almost limitless scaling of production without a significant risk of increasing feedstock or module prices.

Vacuum-deposited CZTS (copper zinc tin sulfide—no selenium) solar cells with 0.66% power conversion efficiency were first reported by Katagiri *et al*. [7]. Optimization of the deposition conditions, metallic precursor concentration, as well as heating and sulfurization conditions has since led to record vacuum-based CZTS power conversion efficiencies of as high as 6.8% [8,9]. Solution-based deposition techniques have also received a great deal of attention because of their potential for lower cost processing. A hydrazine-based route recently led to a record 9.7% power conversion efficiency for the mixed sulfide–selenide CZTSSe materials [6], whereas colloidal nanocrystal-based CZTSSe deposition has led to cells with 7.2% power conversion efficiency [5]. These early results show substantial commercial promise for the kesterite-based class of thin-film photovoltaic materials, especially if the power conversion efficiency could be pushed above 10%.

We report herein the first CZTSSe solar cells with AM1.5 power conversion efficiency above 10%. The absorber layer is deposited by a hydrazine-based liquid process that is amenable to high-throughput roll-to-roll processing [6]. We also present a detailed analysis of the optoelectronic properties of the record device, which enables a useful comparison

with the more mature high-performance CIGSSe solar cell technology.

2. DEVICE FABRICATION AND CHARACTERIZATION

All chemicals were used as-received unless otherwise stated. CZTSSe solutions were prepared as described in a previous publication [6]. Briefly, Cu_2S (synthesized in-house) and S (99.998%; Sigma Aldrich, St. Louis, MO USA) were dissolved in hydrazine (solution A). *Caution: Hydrazine is extremely toxic and explosive and must be handled with appropriate personal protective equipment at all times*. Zn (99.9%; Strem Chemicals, Newburyport, MA USA), SnSe (99.999%; Alfa Aesar, Ward Hill, MA USA), and Se (99.999%, Alfa Aesar) were dissolved in hydrazine separately (solution B). Solutions A and B were combined after all constituents aside from Zn had fully dissolved. The elemental zinc powder reacts to form dispersed $ZnSe(N_2H_4)$ nanoparticle species, thereby leading to a CZTSSe precursor slurry for further processing [6].

To prepare CZTSSe devices, we spin coated five successive layers onto Mo-coated soda lime glass slides using the above-described precursor slurries and heat treated in a sulfur-rich atmosphere using a hot plate temperature setting of as high as 540 °C. Using this approach, well-formed CZTSSe films could be generated with final thickness of ~2.5 μm and a S/(S+Se) ratio of 0.4 ± 0.1, as measured by secondary ion mass spectrometry. The metal composition and phase purity of the absorber layer are similar to that of previously reported devices [6]. CdS buffer, ZnO window, and indium tin oxide layers were subsequently deposited by chemical bath deposition and RF magnetron sputtering, respectively, giving a standard CIGSSe/CZTSSe device structure (see Figure 1(inset)) with a device area of approximately 0.45 cm^2, as defined by mechanical scribing. Ni/Al collector grids, defined using a shadow mask, and a MgF_2 antireflection coating were deposited on top by e-beam evaporation.

Electrical characterization was performed using a Newport solar simulator (Newport Corp., Irvine, CA USA), with simulated air mass 1.5 global (AM1.5G) spectrum and equipped with a closed-loop light stabilization system. For low-temperature measurement, a small liquid nitrogen cryostat unit was inserted under the solar simulator. The J_{sc}–V_{oc} measurement employed an automated continuous neutral density filter under constant solar simulator illumination. The capacitance spectroscopy was carried out with an HP4192A LCR meter (Hewlett-Packard, Palo Alto, CA USA). The quantum efficiency measurement employed a Protoflex system (Protoflex Corp., Centennial, CO USA) equipped with a xenon light source and a monochromator with chopper running at 270 Hz. The time-resolved photoluminescence (TR-PL) measurement was performed on a finished cell using a Hamamatsu time-correlated single photon counting system (Hamamatsu Corp., Bridgewater, NJ USA), utilizing a 532-nm solid state laser with a pulse width of less than 1 ns and a repetition rate of 15 kHz.

3. RESULTS AND DISCUSSION

The *J–V* characteristics, external quantum efficiency (*EQE*), and reflectance spectra of our CZTSSe cell are shown in Figure 1, with the device characteristics provided in detail in Table I. For these measurements, the reflectance properties of the cell have been minimized by employing a MgF_2 antireflection coating, thereby yielding an AM1.5G-weighted average reflectivity of 6.4%. The record power conversion efficiency of 10.1% for the current device has been independently measured and certified by the Newport Technology and Applications Center's Photovoltaic Lab (ISO/IEC 17025 compliant). Also in Table I, a comparison is made between our CZTSSe cell and a reference high-performance (19.5% power conversion efficiency) CIGSSe cell (in this case, with no sulfur) from the National Renewable Energy Laboratory, with essentially the same bandgap [10]. In comparison with the high-performance CIGSSe cell, our CZTSSe cell has a

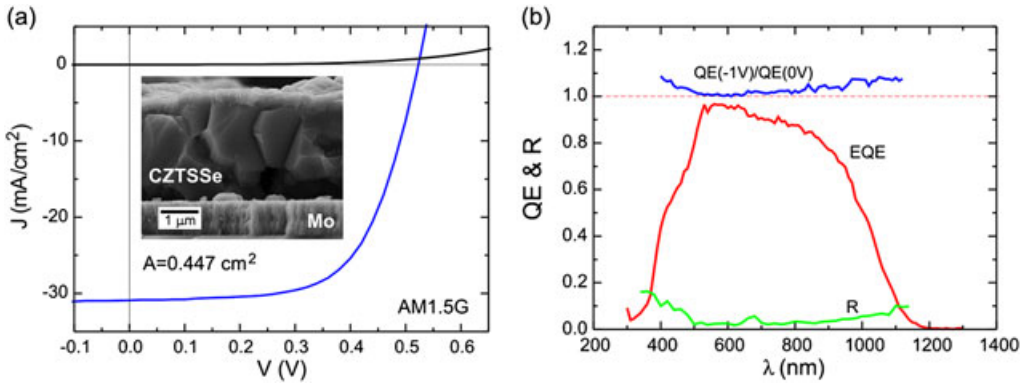

Figure 1. (a) Light and dark *J–V* characteristics at AM1.5G simulated illumination. Inset: SEM cross section of the CZTSSe device. (b) External quantum efficiency (*EQE*) at 0 V bias and reflectance spectra. Top inset: The *EQE* ratio at −1 and 0 V bias.

Table I. Device characteristics for record CZTSSe cell and a reference CIGS cell [10].

	η	FF	V_{oc}	E_g	$E_g/q-V_{oc}$	J_{sc}	R_{SL}	G_{SL}	A	J_0
Cell	(%)	(%)	(mV)	(eV)	(V)	(mA/cm^2)	Ωcm^2	mS/cm^2		mA/cm^2
CZTSSe-1	10.1*	63.7*	517*	1.15	633	30.8*	1.23 (2.47)	0.11	2.0 (1.3)	1.4e−3 (6.6e−6)
CIGS-1	19.5	79.9	692	1.14	448	35.2	0.22	0.17	1.3	3.6e−8

R_{SL}, G_{SL}, A, and J_0 are the series resistance in light, shunt conductance in light, ideality factor, and reverse saturation current determined by the Sites method [11] (and J_{sc}–V_{oc} method in parentheses [12,13]). Note that the discrepancy in the ideality factor between the Sites and J_{sc}–V_{oc} methods is most likely due to non-superposition of light and dark J–V curves.

*Values measured and certified by Newport Corporation (Cert. no. 187, 8 December 2010). The Newport Technology and Applications Center's Photovoltaic Lab is certified by the American Association for Laboratory Accreditation (A2LA) as complying with the international consensus standard ISO/IEC 17025.

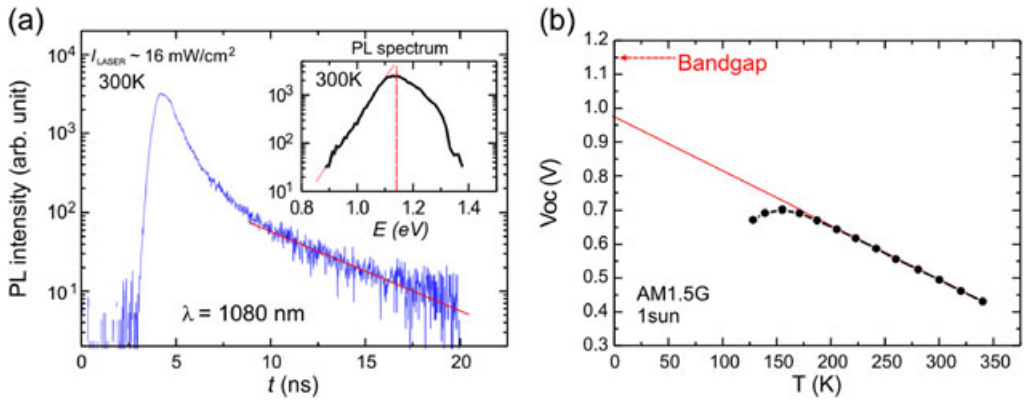

Figure 2. (a) Time-resolved photoluminescence (TR-PL) trace carried out on finished device. Dashed curve is the lifetime fit in the low injection regime. Laser excitation is kept low (~16 mW/cm^2, or 2.8×10^{12} photons/cm^2 per pulse) to avoid distortion of the lifetime measurement. Inset: Room temperature photoluminescence spectrum showing exponential tail (a dashed-line fit) on the lower energy side. The peak (dotted line) is where the TR-PL trace is measured. (b) Temperature dependence of the open-circuit voltage and its linear extrapolation line.

deficiency in open-circuit voltage (25.3%), followed by fill factor (20.3%) and short-circuit current (12.5%), where the numbers in parentheses indicate percentage shortage compared with the CIGSSe device values.

The TR-PL measurement of the cell near band edge emission wavelength (λ=1080 nm) reveals a short minority carrier lifetime, τ=3.1 ns (extracted following the method described in [14]), as shown in Figure 2(a), which is expected to lower V_{oc}. Note that the TR-PL measurement is performed on the finished cell and there could be discrepancies between the lifetime measurement presented here compared with prospective values on the bare absorber layer [15,16]. Accordingly, the measured TR-PL lifetime is expected to give a lower limit to the minority carrier lifetime because of a possible charge separation effect due to the presence of a junction in the completed device [16]. The PL spectrum at room temperature is also presented in the Figure 2(a) inset and shows an emission peak near band edge at E=1.13 eV (λ=1088 nm). This value is consistent with the bandgap extracted from the *EQE* data, which yields E_g=1.15 eV (Table I), following the short diffusion length approximation described in Reference [17]. It should be noted that this bandgap, which can be tuned by varying the degree of sulfurization in the device, falls between the values of 1.21 and 1.03 reported for previous champion cells [18] and coincides with the empirically observed optimum for CIGS cells [10]. The broad band PL emission peak appears asymmetric and is characterized by an exponential tail (indicated by a dashed line) on the low-energy side, which could be related to local fluctuations in the composition or alloy disordering [19].

The deficit in open-circuit voltage (V_{oc}) is apparent in terms of V_{oc} relative to the bandgap value, where $E_g/q-V_{oc}$ =633 mV for our record CZTSSe cell, as compared with only 448 mV for the reference CIGSSe cell. This problem with CZTSSe absorbers has been previously noted for lower-performing devices [20]. Figure 2(b) shows the temperature dependence of V_{oc} for the record CZTSSe cell under AM1.5G illumination. The extrapolation of the linear section to 0 K provides an intercept of E_A=0.97 V, which represents the activation energy of the dominant recombination mechanism. A value equal to the bandgap energy indicates that the dominant recombination mechanism arises in the space charge region. However, E_A falls short

DOI: 10.1002/pip

of the bandgap value of 1.15 eV for the current sample, which indicates a possible dominant interface recombination [21].

The *EQE* in Figure 1(b) appears to be lower in the long wavelength regime, indicating poor carrier collection efficiency in this range and contributing to lower J_{sc}. This carrier collection problem is also indicated by the wavelength dependence of the ratio of *EQE* at −1 and 0 V bias values (Figure 1(b) top inset), where the ratio increases gradually toward long wavelength [22]. Note that low collection efficiency in the long wavelength regime could be attributed to severe back side recombination. However, we believe that short minority carrier lifetime is a more likely limiting factor in our case [20]. The low V_{oc} in our cell (as described above) is also associated with its higher reverse saturation current $J_0 = 1.4 \times 10^{-3}$ mA/cm^2 (Table I). Together with the lower J_{sc}, the increased J_0 accounts for the V_{oc} deficit compared with the reference CIGSSe cell ($\Delta V_{oc} = 179$ mV) according to the following relationship:

$$V_{oc} = AkT/q \ln(J_{sc}/J_0). \quad (1)$$

The short minority carrier lifetime and V_{oc} deficit problem in our device can also be due to a high density of electrical defects. To provide more information on the electrical defect characteristics in our CZTSSe cell, we performed capacitance spectroscopy in the frequency range of 100 Hz–1 MHz, with temperature ranging from 340 to 120 K (Figure 3), following the procedure described in Reference [23]. We observed a defect level centered at 156 meV, similar in position with the N1 defect level commonly found in CIGSSe cells that occurs near 120 meV [24]. This defect level is normally associated with a bulk absorber defect [25]. However, there is no peak near 300 meV as commonly observed in CIGSSe cells [19,26]. The Gaussian fit of this 156 meV defect level yields an integrated defect density of 1.2×10^{15}/cm^3, in the range of the typical 10^{15}/cm^3 integrated defect density level observed in CIGSSe of the same bandgap [26]. Note that despite this similarity in integrated defect density levels, deeper defect levels closer to mid gap, which are beyond the detection limit of our current measurement, may still play an important role in determining minority carrier lifetime and V_{oc} in the CZTSSe devices. These mid-gap traps are currently being studied by transient photocapacitance spectroscopy [27], and the results will be reported in a future publication.

Furthermore, we also extract the carrier density by the drive-level capacitance profiling method, as described in Reference [25] and shown in Figure 3 inset. In general, the carrier density at high (room) temperature is the sum of free carrier density and the defect emission. We determined a carrier density in our CZTSSe cell of ~8×10^{15}/cm^3, which is in the range of typical carrier densities for CIGSSe films [25]. Note that the carrier profile shown in Figure 3 inset starts at 0.3 μm, which is the depletion width at zero bias.

Finally and as we have observed before [18,20], our cell suffers from a relatively low fill factor, which can partly be attributed to the high series resistance (R_S), in turn presumably associated with a potential barrier such as a blocking back contact. The blocking back contact problem is apparent in the diverging series resistance behavior at low temperature as shown in Figure 4, where R_S increases by as much as 400× from 340 to 140 K. Following the model described in Reference [20], the series resistance has the following temperature-dependent behavior:

$$R_S = R_0 + (k/qA^*T) \times \exp(\Phi_B/kT) \quad (2)$$

where A^* is the effective Richardson constant and Φ_B is the blocking contact barrier height. The first term, R_0, is the background series resistance coming from the contact grid and distributed resistance in the transparent conducting oxide

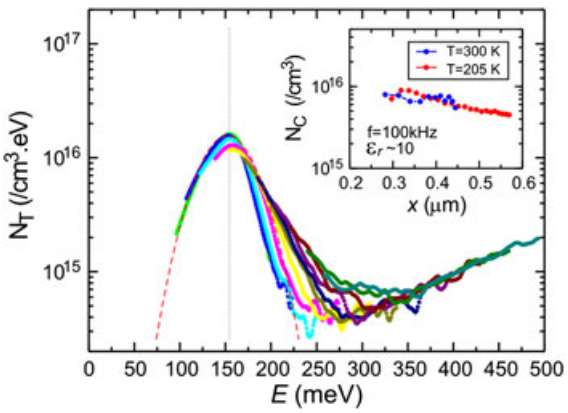

Figure 3. Defect density derived from capacitance spectroscopy (10–1 MHz, 120 to 340 K). The dashed curve is a Gaussian fit to the 156 meV defect level. Inset: Carrier density profile determined from drive-level capacitance profiling technique at 300 and 200 K.

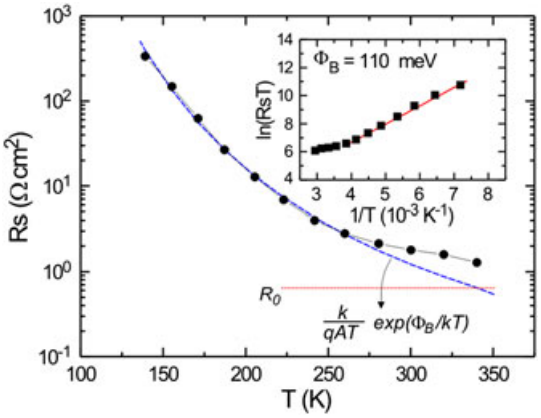

Figure 4. Temperature dependence of the dark series resistance. The dotted line is the residual background series resistance, R_0, and the dashed line is the blocking back contact term. Both components are obtained from curve fitting Equation 2 (see text). Inset: The blocking contact's barrier height determination.

layer, which we assume to be nominally temperature independent. The second term is the Schottky term, based on the thermionic emission model, arising from the blocking back contact.

We obtain the blocking contact barrier height Φ_B=110 meV from the fit of the low-temperature section of the ln (R_sT) versus 1/T plot [20], as shown in Figure 4 inset for our CZTSSe cell. Note that although the differences are quite small, so far we observe that this barrier height tends to increase with the bandgap of the absorber layer (i.e. see Reference [20], where E_g=1.05 and 1.21 eV and the CZTSSe devices yield barrier heights of 99 and 115 meV, respectively), which is consistent with the fact that a Schottky barrier to a p-type material will become higher for a higher bandgap material (assuming that the larger bandgap is mostly accommodated by a shift of the valence band edge). On the basis of the model in Equation 2 and the extracted barrier heights, we can solve for the remaining unknowns R_0 and A^* in Equation 2 and plot the two terms in Equation 2, as shown as dashed curves in Figure 4. Using this approach, a residual background resistance of R_0=0.64 Ωcm^2 is obtained. At 300 K, this leaves 1.8 Ω cm^2 for the series resistance coming from the blocking back contact, which is significant. Thus, the blocking back contact constitutes a significant contribution to the total series resistance at room temperature. Note that, although we here model the barrier assuming a blocking back contact, the barrier could in part be arising elsewhere in the device, such as at the CZTSSe/CdS interface or at grain boundaries.

4. CONCLUSION

We have demonstrated a 10.1% CZTSSe solar cell and presented some essential device characteristics. As observed in earlier samples with lower performance [18,20], the present CZTSSe device suffers from dominant interface recombination, short minority carrier lifetime, and high series resistance. Capacitance spectroscopy reveals a dominant defect level at 156 meV with integrated defect density (~10^{15}/cm^3), similar to that typically found in CIGSSe cells. Indeed, the CZTSSe device reported here is strikingly similar to $CuInSe_2$ devices with 10% power conversion efficiency reported in the past [15,28] in terms of device characteristics (e.g. V_{oc}, J_{sc}, *FF*, free carrier density). Successfully addressing the device shortcomings noted above is expected to enable CZTSSe to achieve further performance gains and to join CIGSSe and CdTe as a commercially viable high-performance solar cell technology.

ACKNOWLEDGEMENTS

We thank S. Jay Chey for the deposition of ZnO and indium tin oxide, R. Ferlita for the Ni/Al evaporation, S. Thiruvengadam for the Cu_2S synthesis, and T. Goislard de Monsabert for the assistance with high-accuracy device area measurement. This work was conducted as part of a joint development project between Tokyo Ohka Kogyo Co., Ltd., DelSolar Co., Ltd., Solar Frontier K. K., and IBM Corporation.

REFERENCES

1. Bhattacharya RN, Contreras MA, Egaas B, Noufi RN, Kanevce A, Sites JR. High efficiency thin-film $CuIn_{1-x}Ga_xSe_2$ photovoltaic cells using a $Cd_{1-x}Zn_xS$ buffer layer. *Applied Physics Letters* 2006; 89:253503 (2 pages).
2. Bosio A, Menossi D, Mazzamuto S, Romeo N. Manufacturing of CdTe thin film photovoltaic modules. *Thin Solid Films*, In Press, doi:10.1016/j.tsf.2010.12.137.
3. Feltrin A, Freundlich A. Material considerations for terawatt level deployment of photovoltaics. *Renewable Energy* 2008; 33:180–185.
4. International Energy Outlook 2010. [cited 2010 January 14]; Available from: www.eia.gov/oiaf/ieo/index.html.
5. Guo Q, Ford GM, Yang WC, Walker BC, Stach EA, Hillhouse HW, Agrawal R. Fabrication of 7.2% efficient CZTSSe solar cells using CZTS nanocrystals. *Journal of the American Chemical Society* 2010; 132:17384–17386.
6. Todorov TK, Reuter KB, Mitzi DB. High-efficiency solar cell with earth-abundant liquid-processed absorber. *Advanced Materials* 2010; 22:E156-E159.
7. Katagiri H, Sasaguchi N, Hando S, Hoshino S, Ohashi J, Yokota T. Preparation and evaluation of Cu_2ZnSnS_4 thin films by sulfurization of E-B evaporated precursors. *Solar Energy Materials and Solar Cells* 1997; 49:407–414.
8. Katagiri H, Jimbo K, Yamada S, Kamimura T, Maw WS, Fukano T, Ito T, Motohiro T. Enhanced conversion efficiencies of Cu_2ZnSnS_4-based thin film solar cells by using preferential etching technique. *Applied Physics Express* 2008; 1:041201 (2 pages).
9. Wang K, Gunawan O, Todorov T, Shin B, Chey SJ, Bojarczuk NA, Mitzi D, Guha S. Thermally evaporated Cu_2ZnSnS_4 solar cells. *Applied Physics Letters* 2010; 97: 143508 (3 pages).
10. Contreras MA, Ramanathan K, AbuShama J, Hasoon F, Young DL, Egaas B, Noufi R. Diode characteristics in state-of-the-art ZnO/CdS/$Cu(In_{1-x}Ga_x)Se_2$ solar cells. *Progress in Photovoltaics: Research and Applications* 2005; 13:209–216.
11. Sites JR, Mauk PH. Diode quality factor determination for thin-film solar cells. *Solar Cells* 1989; 27:411–417.
12. Pysch D, Mette A, Glunz SW. A review and comparison of different methods to determine the series resistance of

solar cells. *Solar Energy Materials and Solar Cells* 2007; 91:1698–1706.
13. Sinton RA, Cuevas A. A quasi-steady-state open-circuit voltage method for solar cell characterization. Proceedings of the 16th European Photovoltaic Solar Energy Conference 2000:1152–1155.
14. Ohnesorge B, Weigand R, Bacher G, Forchel A, Riedl W, Karg FH. Minority-carrier lifetime and efficiency of Cu(In,Ga)Se_2 solar cells. *Applied Physics Letters* 1998; 73:1224 (3 pages).
15. Repins IL, Stanbery BJ, Young DL, Li SS, Metzger WK, Perkins CL, Shafarman WN, Beck ME, Chen L, Kapur VK, Tarrant D, Gonzalez MD, Jensen DG, Anderson TJ, Wang X, Kerr LL, Keyes B, Asher S, Delahoy A, Von Roedern B. Comparison of device performance and measured transport parameters in widely varying Cu (In,Ga)(Se,S) solar cells. *Progress in Photovoltaics: Research and Applications* 2006; 14:25–43.
16. Metzger WK, Repins IL, Contreras MA. Long lifetimes in high-efficiency Cu(In,Ga)Se_2 solar cells. *Applied Physics Letters* 2008; 93:,022110 (3 pages).
17. Zoppi G, Forbes I, Miles RW, Dale PJ, Scragg JJ, Peter LM. $Cu_2ZnSnSe_4$ thin film solar cells produced by selenisation of magnetron sputtered precursors. *Progress in Photovoltaics: Research and Applications* 2009; 17:315–319.
18. Mitzi DB, Gunawan O, Todorov TK, Wang K, Guha S. The path towards a high-performance solution-processed kesterite solar cell. *Solar Energy Materials and Solar Cells* 2011; 95:1421–1436.
19. Burgelman M, Engelhardt F, Guillemoles JF, Herberholz R, Igalson M, Klenk R, Lampert M, Meyer T, Nadenau V, Niemegeers A, Parisi J, Rau U, Schock HW, Schmitt M, Seifert O, Walter T, Zott S. Defects in Cu (In,Ga)Se_2 semiconductors and their role in the device performance of thin-film solar cells. *Progress in Photovoltaics: Research and Applications* 1997; 5:121–130.
20. Gunawan O, Todorov TK, Mitzi DB. Loss mechanisms in hydrazine-processed $Cu_2ZnSn(Se,S)_4$ solar cells. *Applied Physics Letters* 2010; 97:233506 (3 pages).
21. Nadenau V, Rau U, Jasenek A, Schock HW. Electronic properties of $CuGaSe_2$-based heterojunction solar cells. Part I. Transport analysis. *Journal of Applied Physics* 2000; 87:584 (10 pages).
22. Shafarman WN, Klenk R, McCandless BE. Device and material characterization of Cu(InGa)Se_2 solar cells with increasing band gap. *Journal of Applied Physics* 1996; 79:7324 (5 pages).
23. Walter T, Herberholz R, Muller C, Schock HW. Determination of defect distributions from admittance measurements and application to Cu(In,Ga) Se_2 based heterojunctions. *Journal of Applied Physics* 1996; 80:4411 (10 pages).
24. Herberholz R, Igalson M, Schock HW. Distinction between bulk and interface states in $CuInSe_2$/CdS/ZnO by space charge spectroscopy. *Journal of Applied Physics* 1998; 83:318 (8 pages).
25. Heath JT, Cohen JD, Shafarman WN. Bulk and metastable defects in $CuIn_{1-x}Ga_xSe_2$ thin films using drive-level capacitance profiling. *Journal of Applied Physics* 2004; 95:1000 (11 pages).
26. Hanna G, Jasenek A, Rau U, Schock HW. Open circuit voltage limitations in $CuIn_{1-x}Ga_xSe_2$ thin-film solar cells—dependence on alloy composition. *Physica Status Solidi (A)* 2000; 179:R7-R8.
27. Heath JT, Cohen JD, Shafarman WN, Liao DX, Rockett AA. Effect of Ga content on defect states in $CuIn_{1-x}Ga_xSe_2$ photovoltaic devices. *Applied Physics Letters* 2002; 80:4540 (3 pages).
28. Shafarman WN, Phillips JE. Diode analysis of $CuInSe_2$ solar cells. *Proceedings of the 22nd IEEE Photovoltaic Specialist Conference* 1991; 934–939.